Dicrotic Notch Identification: a Generalizable Hybrid Approach under Arterial Blood Pressure (ABP) Curve Deformations

Mahya Saffarpour[1], Debraj Basu[1], Fatemeh Radaei[1], Kourosh Vali[1], Jason Y. Adams[2], Chen-Nee Chuah[1], and Soheil Ghiasi[1]

***Abstract*— Dicrotic Notch (DN) is a distinctive and clinically significant feature of the arterial blood pressure curve. Its automatic identification has been the focus of many kinds of research using either model-based or rule-based methodologies. However, since DN morphology is quite variant following the patient-specific underlying physiological and pathological conditions, its automatic identification with these methods is challenging. This work proposes a hybrid approach that employs both model-based and rule-based approaches to enhance DN detection's generalizability. We have tested our approach on ABP data gathered from 14 pigs. Our result strongly indicates 36% overall mean error improvement with maximum 52% and 11% accuracy enhancement and degradation in extreme cases.**

I. Introduction

DN, the transient increase in the arterial blood pressure curve, is a clinically significant feature that indicates the complete closure of the left ventricle and the end of the systolic duration [1]. The interval between end-diastole and DN (Left Ventricle Ejection Time or LVET) is a primary indicative measure for many conditions such as aortic valve disease, left ventricle muscle failure [2], ischemic heart disease, heart failure, hypertension, and aortic stenosis [3]. Hence the automatic detection of the DN onset and contributing factors is of significance in blood pressure study and monitoring.

The wide-range variability of DN morphology, ranging from a distinct local minimum to a slight change in the waveform slope, makes DN detection challenging. In their pioneering work on pulse waveform analysis, Dawber et al. [4], [5], [6] define four classes for the categorization of arterial pulse waves. They are shown in Fig. 1.

Rule-based and model-based approaches are two general methods previously discussed in the literature for automatic DN detection. Rule-based approaches utilize a set of expert-crafted rules to find the DN location [7], [8], [9], [10], [11]. Model-based approaches, on the other hand, use the underlying differential equations governing the physiological system to explain the pressure signal and spot the DN location [12], [13], [14].

*This work was supported by the National Science Foundation (NSF) Grant No. IIS-1838939, the National Institutes of Health (NIH) award R21HD097467, and the Department of Defense (DoD) CDMRP Grant No. W81XWH1820072.

[1]Mahya Saffarpour, Debraj Basu, Fatemeh Radaei, Kourosh Vali, Soheil Ghiasi, and Chen-Nee Chuah are with the department of Electrical and Computer Engineering, UC Davis, One Shields Ave., Davis, CA, USA (email of the corresponding author: msaff@ucdavis.edu) .

[2]Jason Y. Adams is with the department of Pulmonary and Critical Care Medicine, UC Davis School of Medicine, Sacramento, CA, USA.

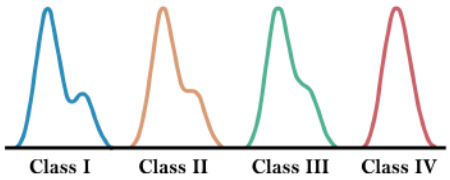

Fig. 1. Various morphologies of the dicrotic notch ([4], [5], [6])

Rule-based algorithms are the dominant approach because of their speed and simplicity. However, their performance is sensitive to blood pressure deformations and limited by the expert knowledge and their competence in designing the rules set. Thus, a rule-based algorithm may fail to generalize in variant deformation occurrences where the DN detection can be challenging.

On the other hand, the model-based approaches can generalize under such unexpected morphology variations as they analyze the underlying physiological system. However, their added complexity and non-convex structure make the optimization convergence sensitive to the optimization methodology and parameter initialization. As a result, their application for DN detection has been limited to normal blood-pressure curves where convergence is achievable.

We propose a generalizable hybrid DN detection approach, with both model-based and rule-based sub-components, that enhances the performance in complex deformed cases where the pure rule-based algorithms fail. In the proposed approach, the rule-based sub-component is entirely separate from the model-based layer and can be substituted by previously proposed rule-based approaches in the field. We have selected two rule-based algorithms that are highly cited and provide open-source detection libraries for testing purposes. These are the work of Pan et al. [15], and Li et al. [16].

We have evaluated the proposed hybrid approach using in-vivo data collected from 14 pigs undergoing sepsis and hemorrhage studies and annotated by expert physicians. The results show up to 36% percent overall improvement in mean DN detection error. When we focus on each gathered dataset separately, the approach shows up to 52% accuracy improvement in the best case while causing -11% accuracy decline in the worst case.

Sections II and III explain the details of the proposed methodology and the results of the approach on the pig dataset. The last section IV is dedicated to the overall conclusion of this paper.

II. Methodology

In this section, we explain the proposed hybrid approach for DN detection. In what follows, we explain the details of the physiological model, the proposed optimization methodology, the hybrid structure, and the evaluation metrics.

A. Cardiovascular Model

Our simplified cardiovascular model is composed of three single-input single-output compartments connected in a closed-loop. These compartments, the left pulsating heart (LPH), arterial systemic compartment (ASC), and post-arterial systemic compartment (PASC), are illustrated in Fig. 2. They contain the simplified hydraulic differential equations governing blood circulation through the cardiovascular system. The details of the LPH are explained in the baseline model [17].

In the baseline model, the heart's pumping pulses are modeled as an output flow source with a single squared sinusoidal pulse during the LVET. We have extended the ventricular output flow source, $F_{o,l}$, to include the DN activation function.

The DN is widely known to be caused by a brief aortic back-flow at the end of ejection duration that fully closes the left ventricle [1]. The effect of aortic back-flow, F_{bf}, is modeled in (1) as a flow source parallel to the $F_{o,l}$. V_{lv} and $F_{i,l}$ are left ventricle's Blood Volume and input blood flow, respectively (details explained in the baseline model).

$$\frac{dV_{lv}}{dt} = F_{i,l} - (F_{o,l} + F_{bf}) \tag{1}$$

F_{bf} in each heart beat duration is then modeled with a Sine-squared function with magnitude, A, duration, T_d, and unset time, T_u, as shown on (2).

$$F_{bf}(t) = \begin{cases} Asin^2(\frac{\pi(t \quad T_u)}{T_d}) & \text{for } t \in [T_u, T_u + T_d] \\ 0 & \text{O.W.} \end{cases} \tag{2}$$

Equations (3) to (6) describe the function of ASC and PASC. In these equations V_t is the total blood Volume. Subscripts ex, sa, pa, and la denote left ventricle exit region, systemic arteries, post-arterial region, and left atrium.

$$\frac{dP_{ex}}{dt} = \frac{1}{C_{sa}}.(F_{o,l} + F_{bf} - F_{sa}) \tag{3}$$

$$\frac{dF_{sa}}{dt} = \frac{1}{L_{sa}}.(P_{ex} - P_{sa} - R_{sa}.F_{sa}) \tag{4}$$

$$\frac{dP_{sa}}{dt} = \frac{1}{C_{pa}}(F_{sa} - \frac{P_{sa} - P_{la}}{R_{pa}}) \tag{5}$$

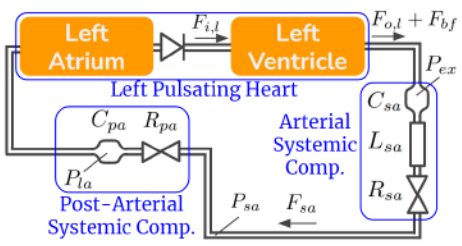

Fig. 2. Three-compartment cardiovascular model.
P: pressures, R: hydraulic resistances, C: compliances, L: inertances

$$P_{la} = \frac{1}{C_{la}}(V_t - C_{sa}P_{ex} - C_{pa}P_{sa} - V_{lv}) \tag{6}$$

B. Optimization Methodology

Parameter estimation of the cardiovascular physiological model is a non-convex problem with no convergence guarantee. The optimizer performance is sensitive to the optimizer settings and the initialization of the parameters.

To mitigate the problem, we guide the parameter estimation using the optimizer cost function and two stages of automatic and case-sensitive parameter initialization. Our proposed approach consists of two consecutive runs of the gradient-based parameter estimation with one stage of parameter initialization at the beginning of each optimizer run.

The cost function is designed to use the prior literature-driven knowledge on physiological parameters values to limit the search space of the parameter estimation and improve the convergence.

The initialization stages are also purposefully designed to help the optimizer to, first, find the general placement of the simulated arterial pressure signal at the first stage and, then, fine-tune the back-flow parameters for DN identification at the second stage.

In this section, we detail the parameter estimation methodology (similar in both stages) and explain the initialization of the parameters of each stage.

1) Parameter Estimator: The proposed parameter estimator calculates the gradient of its cost function H for each parameter value using a local sensitivity analysis algorithm. The proposed cost function (7) minimized the sum of two separate weighted terms. They are the squared error of the estimated pressure and squared parameters displacement at each iteration step j. The displacement term limits the parameters search space by increasing the cost with squared distance from the average value and improving the convergence.

$$H_j = ||W_d(P_{e_j} - \overline{P}_p) \odot {\overline{P}_p}^{-1}||^2 + ||W_e(Y_{e_j} - Y_m)||^2 \tag{7}$$

where P_e, $\overline{P}_p$, Y_e, and Y_m are estimated parameters vector, parameters average value vector, estimated arterial pressure, and measured arterial pressure respectively. W_d and W_e are the weight vectors of the displacement and error terms.

In order to magnify the systolic and diastolic blood pressures in the cost function, W_e is increased during systolic and diastolic peaks. These peaks are pinpointed on the measurement curve, and their indices are fed into the cost function's weight generator ahead of the optimization initiation.

For the cost function's gradient calculation, we have selected the continuous local sensitivity analysis (CSA) method [18] considering the relatively small number of parameters under optimization (less than 100) and its timing benefits.

The forward-mode of CSA calculates the model sensitivities by extending the ODE system to include (8); where $\frac{\partial f}{\partial u}$ is the Jacobian of the derivative function f with respect to the current state variable, u, and $\frac{\partial f}{\partial p_i}$ is the gradient of the derivative function concerning the i-th parameter.

$$\frac{d}{dt}(\frac{\partial u}{\partial p_i}) = \frac{\partial f}{\partial u}\frac{\partial u}{\partial p_i} + \frac{\partial f}{\partial p_i} \tag{8}$$

TABLE I

STAGE I: PARAMETERS INITIALIZATION

Initial values driven from [17]				
Compliance, $(ml/mmHg)$	Hydraulic Resistance, $(mmHg.s.ml^{-1})$	Inertance, $(mmHg.ml.s^{-2})$		Volume (ml)
$C_{sa} = 0.52$ $C_{pa} = 0.52$	$R_{sa} = 0.529$ $R_{pa} = 0.529$	$L_{sa} = 0.22.10^{-3}$		$V_t = 5300$
Problem-specific initial values				
Pressure, $(mmHg)$	Flow, $(ml.s^{-1})$	Volume, (ml)	Time, (s)	Amplitude
$P_{sa,0} = 60$ $P_{ex,0} = 30$	$F_{sa,0} = 5$	$V_{lv,0} = 225$	$T_d = 0.02$ $T_u = 0.1$	$A = 10$

2) First Stage Initialization: As mentioned before, the first stage optimization imitates the general positioning and morphology of the blood pressure curve. At the same time, the cost function displacement term keeps the parameters in the expected physiological range.

Therefore, at the beginning of the first stage, the parameters are initialized to their average values ($\overline{P}_p$), derived from clinical literature [17]. For parameters with no prior expected values, we have picked the initial values based on the optimizer's stability through several algorithm runs.

Table I lists the initialization of the parameters for the first stage.

3) Second Stage Initialization: During the second stage initialization, the estimated parameters from the first stage optimization are altered to magnify the DN peak in the estimated waveform. This way, a high DN peak is imposed on the previously estimated arterial pressure in stage one. The optimizer is guided out of the local minima to focus on DN shape and location during the second stage parameter estimation.

The case-sensitive parameter alteration (9) is applied to the backflow parameters to affect the DN shape and location.

$$Tu = \frac{2}{3}T_{hb}, \quad A = 50 \tag{9}$$

where T_{hb} is the heart-beat time period.

C. Hybrid Approach

The hybrid approach combines the proposed model-based method with the existing rule-based methodologies to improve the DN detection under blood pressure deformations.

Our proposed model-based approach is first applied to the data to estimate an approximate version of the blood pressure curve with reduced deformation. The estimated blood pressure is then passed through the pre-existing rule-based algorithms to identify the DN placement.

To improve the performance, we have also designed a voting method. If both rule-based and hybrid algorithms have placed a DN location for a heartbeat, the average position is identified as the voting result. Otherwise, if one failed to find a DN location in a heartbeat under study, the result of the remaining algorithm decides the DN position.

D. Evaluation Metrics

We define error of DN detection in each heartbeat time-series, b, to be the absolute time difference between the gold-standard and detected DN location in each heart beat (10).

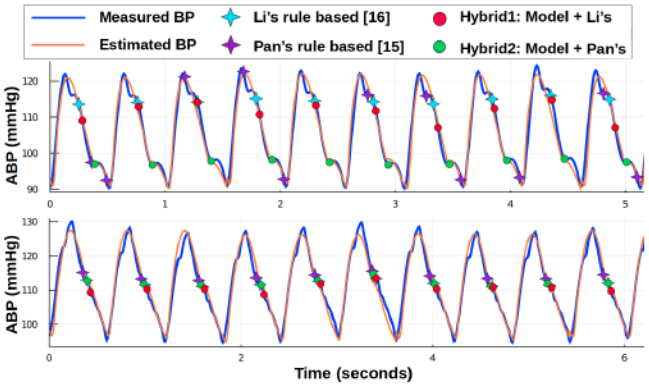

Fig. 3. Different methods applied to detect DN in two examples of swine ABP waveform

$$Err_b = |T_{detected} - T_{gold}| \tag{10}$$

Using the aforementioned heartbeat-level definition of Err, (11) presents the defined DN detection accuracy percentage, $Acc_{D_i}\%$, in a dataset, D_i, containing a vector of hearbeats, B_i, under a maximum permitted error, E_M.

$$Acc_{D_i}\% = \frac{100 \times card(\{b_{i,j} \in D_i | Err_{b_{i,j}} \leq E_M\})}{card(D_i)} \tag{11}$$

where $card(D_i)$ stands for the cardinality of set D_i.

III. RESULTS

We have implemented the cardiovascular model, and the parameter estimator using the Julia Language and special libraries [19], [20], [21], [22]. The estimator uses the ADAM optimizer [23] with a learning rate equal 0.01 and first and second decay of momentums equal 0.9 and 0.999 consecutively.

We have analyzed ABP signals for 24 datasets randomly selected from 4 and 10 pigs undergoing sepsis and hemorrhage studies, respectively, for our experimental demonstration. Each dataset contains 27 heartbeats and 648 heartbeats in total. All the DNs are manually annotated by an expert physician. These annotations are the gold standard against which the performance will be compared. The dataset sampling frequency is 100 Hz.

We went through the rigorous preprocessing method to remove noise and other artifacts from the signal using Savitzky-Golay (S-G) filters [24]. The S-G filter is a moving average filter to smooth the arterial blood pressure signal. It was selected due to the advantage of sharp edge preservation [25]. We present our results on two datasets in Fig. 3 as example plots.

Table II provides statistics of DN detection quality under different methods. The results show that the hybrid approach with voting can improve the mean error by 36% while reducing its standard deviation by 41%. It also gains up to 52% accuracy improvement in the best case with only -11% decline in the worst case.

TABLE II

DN DETECTION STATISTICS UNDER DIFFERENT METHODS

	Overall Err statistics		Acc%, $E_M = 50ms$		
Method	Mean, (ms)	SD, (ms)	Total	Best Dset improv.	Worst Dset improv.
Li's RB [16]	49	37	63%	—	—
Hybrid: M+Li's	49	30	60%	93%	-74%
Voting: Hyb.+Li's	42	31	70%	93%	-70%
Pan's RB [15]	42	61	86%	—	—
Hybrid: M+Pan's	29	39	90%	89%	-22%
Voting: Hyb.+Pan's	27	36	91%	52%	-11%

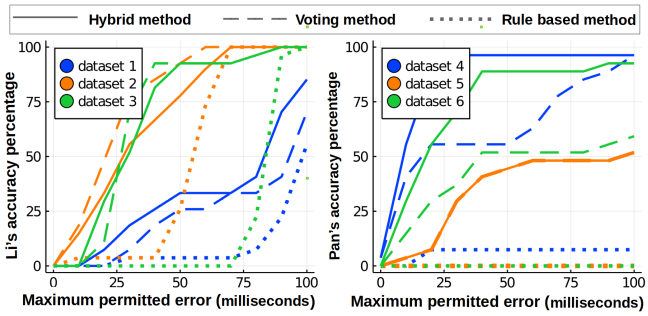

Fig. 4. Accuracy of the proposed DN detection approaches applied to 27 heartbeat datasets that are hard cases for each baseline rule based method

In this paper, we consider hard datasets for a specific rule-based algorithm to be the ones with an $Acc\% \leq 50\%$ under $E_M = 50ms$. In other words, a dataset is hard for a rule-based algorithm if the algorithm cannot find the DN location of more than 50% of its heartbeats with $Err_s \leq 50ms$.

The DN detection evaluation of 24 datasets finds 10 and 3 hard cases for Li's [16] and Pan's [15]. We then select three hard cases for each rule-based algorithm, dataset 1-3 for Li's and 4-6 for Pan's algorithm, and apply our proposed DN detection approaches to test the accuracy level for a varying E_M. As shown in Fig. 4, the hybrid and voting methods are strong candidates to deal with real-world ABP signals prone to noise and artifacts.

IV. Conclusion

In this work, we have proposed a hybrid methodology with a generalizable DN detection capability in the presence of many typical blood pressure curve deformations. The method has shown 36% mean error improvement on real-world expert-annotated pig data undergoing sepsis and hemorrhage study.

References

[1] A. Guyton and J. Hall, "Textbook of medical physiology, 11th," 2006.

[2] R. P. Lewis, S. Rittogers, W. Froester, and H. Boudoulas, "A critical review of the systolic time intervals." *Circulation*, vol. 56, no. 2, pp. 146–158, 1977.

[3] T. Biering-Sørensen, G. Querejeta Roca, S. M. Hegde, A. M. Shah, B. Claggett, T. H. Mosley Jr, K. R. Butler Jr, and S. D. Solomon, "Left ventricular ejection time is an independent predictor of incident heart failure in a community-based cohort," *European journal of heart failure*, vol. 20, no. 7, pp. 1106–1114, 2018.

[4] T. R. Dawber, H. E. THomas Jr, and P. M. McNamara, "Characteristics of the dicrotic notch of the arterial pulse wave in coronary heart disease," *Angiology*, vol. 24, no. 4, pp. 244–255, 1973.

[5] S. C. Millasseau, J. M. Ritter, K. Takazawa, and P. J. Chowienczyk, "Contour analysis of the photoplethysmographic pulse measured at the finger," *Journal of hypertension*, vol. 24, no. 8, pp. 1449–1456, 2006.

[6] T. Tigges, Z. Music, A. Pielmus, M. Klum, A. Feldheiser, O. Hunsicker, and R. Orglmeister, "Classification of morphologic changes in photoplethysmographic waveforms," *Current Directions in Biomedical Engineering*, vol. 2, no. 1, pp. 203–207, 2016.

[7] A. Chakraborty, D. Sadhukhan, and M. Mitra, "Accurate detection of dicrotic notch from ppg signal for telemonitoring applications," *Int J Biomed Eng Technol*, 2018.

[8] O. Singh and R. K. Sunkaria, "Detection of onset, systolic peak and dicrotic notch in arterial blood pressure pulses," *Measurement and Control*, vol. 50, no. 7-8, pp. 170–176, 2017.

[9] J. Balmer, R. Smith, C. G. Pretty, T. Desaive, G. M. Shaw, and J. G. Chase, "Accurate end systole detection in dicrotic notch-less arterial pressure waveforms," *Journal of clinical monitoring and computing*, pp. 1–10, 2020.

[10] A. Donelli, J. R. Jansen, B. Hoeksel, P. Pedeferri, R. Hanania, J. Bovelander, F. Maisano, A. Castiglioni, O. Alfieri, and J. J. Schreuder, "Performance of a real-time dicrotic notch detection and prediction algorithm in arrhythmic human aortic pressure signals," *Journal of clinical monitoring and computing*, vol. 17, no. 3, pp. 181–185, 2002.

[11] B. N. Li, M. C. Dong, and M. I. Vai, "On an automatic delineator for arterial blood pressure waveforms," *Biomedical Signal Processing and Control*, vol. 5, no. 1, pp. 76–81, 2010.

[12] M. T. Politi, A. Ghigo, J. M. Fernández, I. Khelifa, J. Gaudric, J. M. Fullana, and P.-Y. Lagrée, "The dicrotic notch analyzed by a numerical model," *Computers in biology and medicine*, vol. 72, pp. 54–64, 2016.

[13] T. Myers, V. R. Ripoll, A. S. de Tejada Cuenca, S. L. Mitchell, and M. J. McGuinness, "Modelling the cardiovascular system for assessing the blood pressure curve," *Mathematics-in-industry case studies*, vol. 8, no. 1, pp. 1–16, 2017.

[14] S. Hoeksel, J. Jansen, J. Blom, and J. J. Schreuder, "Detection of dicrotic notch in arterial pressure signals," *Journal of clinical monitoring*, vol. 13, no. 5, pp. 309–316, 1997.

[15] J. Pan and W. J. Tompkins, "A real-time qrs detection algorithm," *IEEE Transactions on Biomedical Engineering*, vol. BME-32, no. 3, pp. 230–236, 1985.

[16] B. N. Li, M. C. Dong, and M. I. Vai, "On an automatic delineator for arterial blood pressure waveforms," *Biomedical Signal Processing and Control*, vol. 5, no. 1, pp. 76–81, 2010. [Online]. Available: https://www.sciencedirect.com/science/article/pii/S1746809409000470

[17] M. Ursino, "Interaction between carotid baroregulation and the pulsating heart: a mathematical model," *American Journal of Physiology-Heart and Circulatory Physiology*, vol. 275, no. 5, pp. H1733–H1747, 1998.

[18] C. Rackauckas, Y. Ma, V. Dixit, X. Guo, M. Innes, J. Revels, J. Nyberg, and V. Ivaturi, "A comparison of automatic differentiation and continuous sensitivity analysis for derivatives of differential equation solutions," *arXiv preprint arXiv:1812.01892*, 2018.

[19] M. Innes, E. Saba, K. Fischer, D. Gandhi, M. C. Rudilosso, N. M. Joy, T. Karmali, A. Pal, and V. Shah, "Fashionable modelling with flux," *CoRR*, vol. abs/1811.01457, 2018. [Online]. Available: http://arxiv.org/abs/1811.01457

[20] C. Rackauckas and Q. Nie, "Adaptive methods for stochastic differential equations via natural embeddings and rejection sampling with memory," *Discrete and continuous dynamical systems. Series B*, vol. 22, no. 7, p. 2731, 2017.

[21] M. Innes, "Flux: Elegant machine learning with julia," *Journal of Open Source Software*, 2018.

[22] C. Rackauckas and Q. Nie, "Differentialequations. jl–a performant and feature-rich ecosystem for solving differential equations in julia," *Journal of Open Research Software*, vol. 5, no. 1, 2017.

[23] D. P. Kingma and J. Ba, "Adam: A method for stochastic optimization," *arXiv preprint arXiv:1412.6980*, 2014.

[24] R. W. Schafer, "What is a savitzky-golay filter? [lecture notes]," *IEEE Signal Processing Magazine*, vol. 28, no. 4, pp. 111–117, 2011.

[25] R. W. Schafer, "On the frequency-domain properties of savitzky-golay filters," in *2011 Digital Signal Processing and Signal Processing Education Meeting (DSP/SPE)*, 2011, pp. 54–59.